Macromolecules

Article

pubs.acs.org/Macromolecules

Nanostructural Evolution and Self-Healing Mechanism of Micellar Hydrogels

Volkan Can,[†] Zdravko Kochovski,[‡] Valentin Reiter,[‡] Nikolai Severin,[‡] Miriam Siebenbürger,[†] Ben Kent,[†] Justus Just,[†] Jürgen P. Rabe,[‡] Matthias Ballauff,[†,‡] and Oguz Okay*[,†,§]

[†]Soft Matter and Functional Materials, Helmholtz-Zentrum Berlin, Hahn-Meitner-Platz 1, D-14109 Berlin, Germany

[‡]Department of Physics & IRIS Adlershof, Humboldt-Universität zu Berlin, Newtonstr. 15, D-12489 Berlin, Germany

[§]Department of Chemistry, Istanbul Technical University, Maslak, 34469 Istanbul, Turkey

Supporting Information

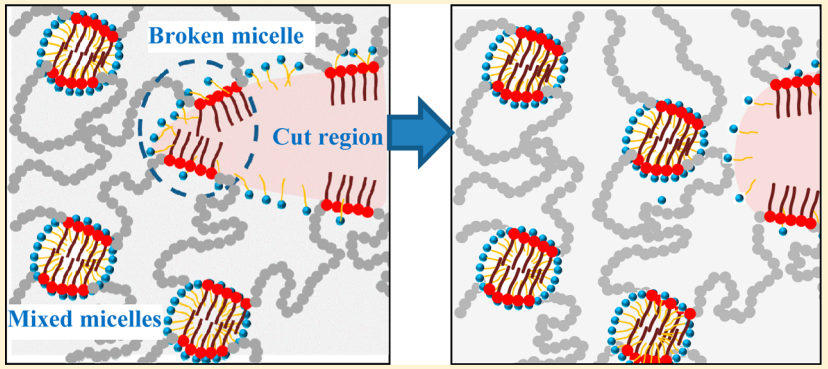

ABSTRACT: Understanding the nanoscale structure and dynamics of supramolecular hydrogels is essential for exploiting their self-healing mechanisms. We describe here nanostructural evolution and self-healing mechanism of hydrogels formed from *in situ* generated hydrophobically modified hydrophilic polymers and wormlike sodium dodecyl sulfate (SDS) micelles. We observe a conformational transition in wormlike SDS micelles upon addition of hydrophobic as well as hydrophilic monomers. Several hundred nanometer long SDS micelles completely disappear after the monomer addition, in favor of spherical micelles with a radius of 2.4 nm. After conversion of the monomers to hydrophobically modified polymer chains via micellar copolymerization, the spherical shape of the micelles remains intact but the radius increases to 2.8 nm. The interconnected spherical mixed micelles consisting of SDS and hydrophobic blocks of the polymer self-assemble to form a layered hydrogel structure. Self-healing response of the damaged hydrogel samples begins by reshaping the injured area into circular holes and ends by complete healing due to the intra- and interlayer mobility of the mixed micelles, respectively.

INTRODUCTION

Certain surfactant micelles are known to self-assemble in aqueous salt solutions into wormlike micelles (WLMs), which can display high viscoelasticity and remarkable stimuli-responsive rheological properties.[1−5] WLMs are similar to classical flexible polymers while they differ from them because of their constantly breaking and recombining events within the reptation time. Addition of a hydrophobically modified hydrophilic polymer to the solution of WLMs can significantly enhance the zero-shear viscosity of the solution, at concentrations that neither the WLM alone nor the polymer can do.[6−12] The greatly enhanced viscoelastic response of aqueous WLM−polymer systems is due to the intercalation of hydrophobic blocks of polymer into the micellar core, thus bridging them to a viscous solution or a physical gel. The living nature of WLMs and enhanced mechanical performance of WLM−polymer systems open up a versatile approach for designing novel soft and smart materials with changeable physical properties—a requirement for self-healing and shape memory effects. Moreover, micellar hydrogels formed by thermogelling of amphiphilic block copolymers in water attract interest as unique biomedical materials.[13−16]

We recently presented a simple strategy to generate self-healing hydrogels comprising *in situ* generated hydrophobically modified hydrophilic polymers and WLMs in the semidilute regime.[17−20] A hydrophobic monomer with a long alkyl side chain such as stearyl methacrylate (C18M) is first solubilized within wormlike sodium dodecyl sulfate (SDS) micelles and then copolymerized with a hydrophilic monomer in aqueous surfactant solution by free radical mechanism. Copolymerization of the monomers via micellar polymerization generates dynamic hydrophobic associations between the hydrophobic domains of polymer chains and surfactant micelles acting as physical cross-links of the resulting hydrogels.[17,18,21,22] These

Received: January 22, 2016
Revised: February 20, 2016
Published: February 29, 2016

DOI: 10.1021/acs.macromol.6b00156
Macromolecules 2016, 49, 2281−2287

reversible breakable cross-links are responsible for rapid self-healing of the hydrogels without the need for any stimulus or healing agent.[17,18] Because the hydrogels exhibit unique characteristics such as insolubility in water but solubility in surfactant solutions, nonergodicity, and a high degree of toughness, they attracted interest in the past several years.[23−25]

However, the evolution of the nanoscale structure during the formation of micellar hydrogels and the mechanism of self-healing are not understood yet. We describe here a complete picture of the nanostructural evolution and self-healing mechanism of micellar hydrogels as depicted in Figures 1a−d.

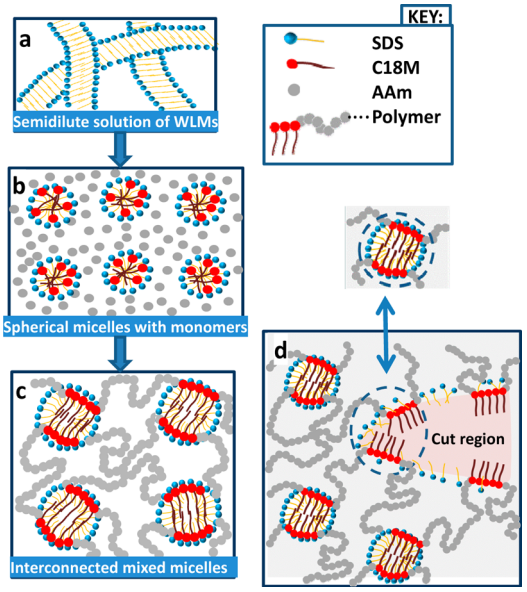

Figure 1. Cartoon showing the formation of micellar hydrogels (a−c) and their self-healing mechanism (d). The double arrow in (d) indicates the gel region before and after healing.

Several hundred nanometer long WLMs with a radius of 1.6 nm first transform into spherical SDS micelles with a radius of 2.4 nm upon dissolution of the hydrophobic monomer C18M and/or hydrophilic monomer acrylamide AAm (a → b). After micellar copolymerization, the interconnected mixed micelles formed preserve their shape while they assume a layered structure in the hydrogel (c). After damaging the hydrogel to create nanosized trenches on the gel surface, the trenches first reshape into circular holes, and then the gel completely self-heals due to the intra- and interlayer mobility of the mixed micelles (d → c).

RESULTS AND DISCUSSION

Conformational Transition in WLMs. We have prepared the pregel solutions at 35 °C and at a SDS concentration of 243 mM, which is above the overlap concentration of SDS micelles.[26] To solubilize the hydrophobic monomer C18M in this micellar solution, NaCl has to be added in amounts between 0.3 and 1 M to induce the micellar growth. Figure 2a shows the zero-shear viscosity η_0 of 243 mM SDS solution plotted against the added amount of NaCl (for details, see Supporting Information and Figure S1). η_0 remains rather low until a NaCl concentration of about 0.5 M but then dramatically increases due to the weakening of electrostatic interactions causing the micelles to grow. The grown SDS micelles possess stimuli-responsive rheological properties. Even

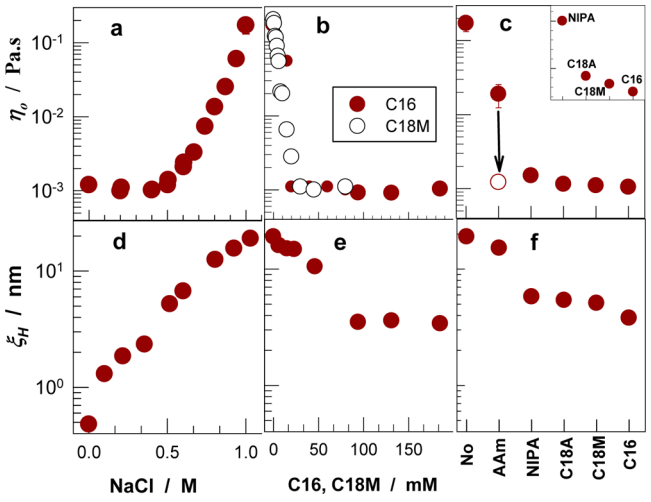

Figure 2. Zero-shear viscosities η_0 (a−c), and hydrodynamic correlation lengths ξ_H (d−f) of 243 mM SDS solutions at 35 °C. Effects of the addition of NaCl, hydrophobes at 1 M NaCl, and several additives (130 mM) at 1 M NaCl are shown. Open symbol in (c) indicates the effect of AAm at 1.29 M.

visual examination of the micellar solutions showed that hydrophobic additives reduce drastically their viscosities, probably due to the oil-induced structural change of wormlike micelles.[27−31] Figure 2b shows the zero-shear viscosity η_0 of 243 mM SDS in 1 M NaCl solution plotted against the added amounts of *n*-hexadecane (C16), a model hydrophobic compound, and the hydrophobic monomer stearyl methacrylate (C18M). η_0 rapidly decreases after addition of the hydrophobes, and at a level above 20 mM, it becomes close to the viscosity of 243 mM SDS in water. A similar but different extent of decrease in η_0 was observed upon addition of acrylamide (AAm), *N*-isopropylacrylamide (NIPA), and *n*-octadecyl acrylate (C18A) to this SDS−NaCl solution. Figure 2c showing a comparison of η_0 of the solutions containing 130 mM of these additives reveals that the higher the hydrophobicity of the additive the larger is the drop in the viscosity. However, the addition of a larger amount of hydrophilic compounds induced similar effect as the addition of the hydrophobes at a small amount. For instance, the open symbol in Figure 2c indicates η_0 of the micellar solution containing 1.29 M AAm. The hydrophilic monomer AAm at this concentration reduces the viscosity to the level of the viscosity of 243 mM SDS in water.

Figures 2d−f show the hydrodynamic correlation lengths ξ_H of 243 mM SDS solutions evaluated from the time average intensity correlation functions (ICFs) at nine scattering angles between 50° and 130°, plotted against the added amount and the type of the additives (see Supporting Information and Figures S2−S4). ξ_H increases with the addition of NaCl and becomes 20 nm at 1 M NaCl, while it again decreases upon addition of *n*-hexadecane or other additives down to 3 nm. This means that the size of the micelles decreases after solubilization of these additives, but the resulting micelles are larger than the monomeric micelles.

The results suggest a conformational transition in grown SDS micelles upon addition of the hydrophobes. To visualize this transition, direct images of vitrified surfactant solutions were obtained by cryo-electron microscopy (cryo-EM). Figure 3a presents cryo-EM micrograph of the vitrified 243 mM SDS in 1 M NaCl solution, while Figure 3b shows the same sample after

DOI: 10.1021/acs.macromol.6b00156
Macromolecules 2016, 49, 2281−2287

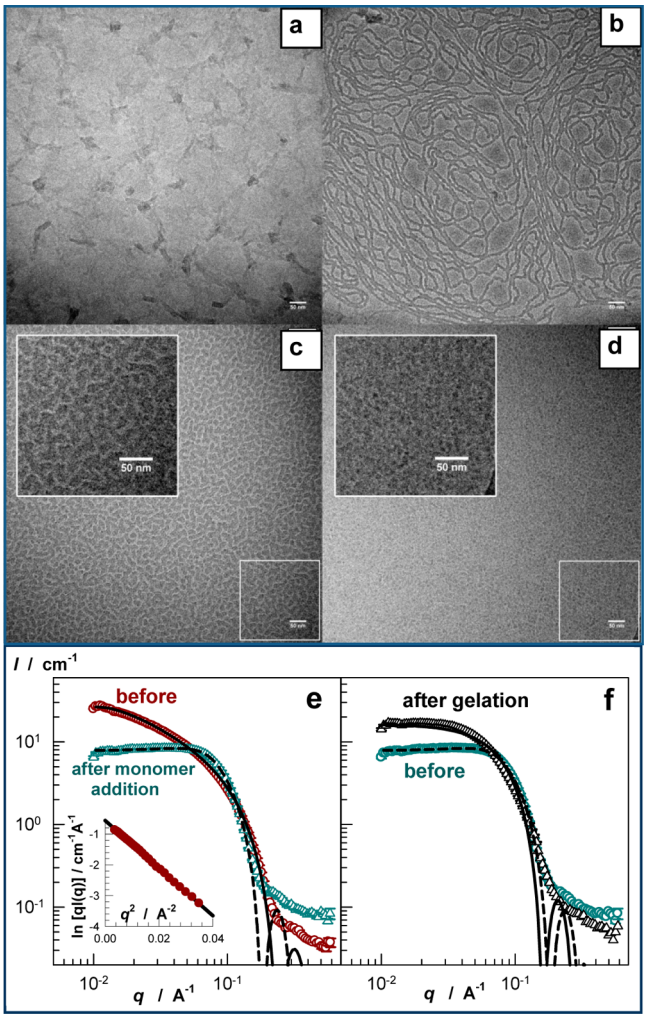

Figure 3. (a–d) Cryo-EM micrographs of surfactant solutions. Scale bars = 50 nm. (a, b) 243 mM SDS in 1 M NaCl solution before (a) and after 1:10 dilution with 1 M NaCl (b). (c, d) 243 mM SDS in 1 M NaCl solution after addition of 130 mM *n*-hexadecane (c), and the monomers AAm (1.29 M) + C18M (26.3 mM) (d). (e, f) SANS profiles for 243 mM SDS in 1 M NaCl solution at 35 °C. (e) Solution before and after monomer addition. The solid and dashed curves are best fits to a form factor of wormlike micelles and spheres, respectively. Inset: $\ln[I(q)q]$ vs q^2 plot for the solution before the monomer addition in the range of q = 0.06–0.19 Å^{-1}. (f) Solution containing the monomers AAm (1.29 M) and C18M (26.3 mM) before and after gelation. The curves are best fits to a form factor of spheres with a radius of 2.4 nm (before gelation) and 2.8 nm (after gelation).

1:10 dilution with 1 M NaCl. After dilution, several hundred nanometer long wormlike SDS micelles are seen, while, before dilution, they overlap and become entangled and aligned due to the high SDS concentration. The alignment of overlapped WLMs can better be observed after 1:5 dilution of the solution (Figure S5). Figure 3c represents the same sample as in Figure 3a, but after addition of 130 mM *n*-hexadecane (C16). Wormlike SDS micelles completely disappear upon addition of the hydrophobe and a system consisting of monodisperse spheres appears. This clearly demonstrates the occurrence of a conformational transition from wormlike to spherical SDS micelles.

In Figure 3d, instead of C16, 1.29 M acrylamide (AAm) together with 26.3 mM stearyl methacrylate (C18M) was added to the wormlike SDS solution. We have to mention that this is the gelation solution to obtain self-healing hydrogels at a monomer concentration of 10% w/v composed of 2 mol % C18 M and the rest being AAm.[18] No wormlike micelles can be detected in this micrograph and spherical micelles with smaller sizes appear after the monomer addition. The drop in η_0 and ξ_H upon dissolution of the additives is thus due to this conformation transition in the micellar structure. This structural change likely occurs due to the accumulation of the hydrophobic monomers in the core of wormlike SDS micelles, which would increase the curvature of the micelle making cylinder–sphere transition in micellar shape favorable.

The conformational transition in SDS micelles upon addition of the hydrophobes was also demonstrated by small-angle neutron scattering (SANS) measurements. The solvent water was substituted with D_2O, and the measurements were performed at the time-of-flight SANS-beamline V16 at the Helmholtz Zentrum Berlin (HZB).[32] Neutrons of wavelength λ = 1.8–6.9 Å were used with a distribution $\Delta\lambda/\lambda$ = 10%. Figure 3e shows the scattering curves obtained for wormlike SDS micellar solutions (243 mM SDS–1 M NaCl) before and after addition of the monomers AAm (1.29 M) and C18M (26.3 mM). Before addition, the intensity I at low scattering vector q increases revealing the presence of long scattering objects. The inset to the figure showing $\ln[Iq]$ vs q^2 plot in the range of q = 0.06–0.19 Å^{-1} is linear characteristics of cylindrical structures. From the slope of this line, the cross-sectional radius of the structure was calculated as 1.76 nm, a value comparable to the extended length of C12 chain (1.67 nm).[33,34] This result supports one-dimensional growth of SDS micelles leaving the cylindrical cross section unaltered. The solid curve in Figure 3e represents the fit of the full neutron scattering data to a form factor of wormlike micelles using SASfit software yielding a cross-sectional radius of 1.60 nm. Figure 3e also shows that the addition of the monomers significantly affects the shape of the scattering curve. The data after the monomer addition could be fitted to monodisperse spheres with a radius of 2.4 nm (dashed curve).

The rheological data in Figures 2c already indicate that the conformation transition in WLMs also occurs upon addition of larger amounts of the hydrophilic monomer acrylamide (AAm). To check this, SANS measurements were conducted after addition of the hydrophilic monomer AAm alone at a concentration of 1.29 M. Similar to the addition of both AAm (1.29 M) and C18 M (26.3 mM), a good fit of the neutron scattering data to monodisperse spheres was obtained while the radius decreased from 2.4 to 1.8 nm (Figure S6). Because of the interactions between hydrophobic double bonds of AAm and SDS, AAm may accumulate around the surfactant palisade layer causing an increase in curvature of WLMs and, by this way, favors cylinder-to-sphere transition. A recent work indeed shows that although polyacrylamide does not interact with SDS, AAm affects its micellar structure by decreasing the aggregation number from 60 in water to 20 in >0.2 M AAm solutions.[35]

Micellar Hydrogels and Self-Healing Mechanism. After micellar polymerization, the monomers are converted into hydrophobically modified hydrophilic polymer chains so that a hydrogel forms with mixed micelles as physical cross-links. The question is, does the spherical shape of the micelles remain intact, or does it return to the initial cylindrical shape? To clarify this, the micellar solution containing the monomers AAm and C18M was subjected to micellar polymerization at 35 °C by the addition of ammonium persulfate (3.5 mM)–

DOI: 10.1021/acs.macromol.6b00156
Macromolecules 2016, 49, 2281–2287

N,N,N′,N′-tetramethylethylenediamine (0.25 v/v %) redox initiator system. SANS measurements were performed after a reaction time of 6 h where a transparent gel was formed. Figure 3f compares SANS profiles before and after the micellar polymerization. The shape of the curves remains almost unchanged indicating that the conversion of the monomers to hydrophobically modified polymer does not affect the spherical shape of the micelles formed after the conformational transition. Another point seen from Figure 3f is the enhanced scattering of the hydrogel at low scattering vectors which we attribute to the spatial inhomogeneities commonly observed in gels with static concentration fluctuations.[36,37] The fit of the neutron scattering data of the hydrogel to monodisperse spheres leads to a radius of 2.8 nm as compared to 2.4 nm before the micellar polymerization. This increase in the micellar radius is reasonable considering the fact that the core radius of spherical micelles is dictated by the maximum length of the hydrophobic tail.[38,39] SANS measurements were repeated by decreasing NaCl concentration from 1.0 to 0.5 M. The cross-sectional radius of wormlike SDS micelles remained unchanged, supporting the fact that the radius of monomeric micelles does not change during the micellar growth (Figure S7). After their conformational transition, the size of the spherical micelles reduced by 10−20%, which is attributed to the decreasing aggregation number of the micelles at lower salt concentrations.

It follows from the above findings that the evolution of micellar hydrogels starting from semidilute solutions of wormlike SDS micelles occurs as depicted in Figure 1a−c. Several hundred nanometer long WLMs first transform into spherical micelles with a radius of 2.4 nm upon dissolution of the monomers. The shape of the micelles remains intact after the hydrogel formation while their radius increases to 2.8 nm. The interconnected mixed micelles composed of hydrophobic groups of C18M units and SDS molecules can be considered as similar to nanosized oil droplets interconnected by coiled hydrophilic polymer chains in a polar gel phase. Frequency sweep data of the hydrogel measured at a strain amplitude γ_0 of 1% indicate temporary nature of the mixed micelles with lifetimes of the order of seconds to milliseconds (Figure 4a). Figure 4b shows five successive cycles of high (3−300%) to low (1%) oscillatory strain amplitudes and the resulting elastic modulus G' vs time plot. The hydrogel recovers its original modulus (9 kPa) and loss factor tan δ (0.2, not shown) almost instantaneously upon reducing the strain to 1%, demonstrating reversible dissociation−associations of the mixed micellar cross-links.

Figure 4c shows typical ICFs of the hydrogel obtained with different acquisition times at a scattering angle of 90° and the distributions of the relaxation rates $G(\Gamma)$. Very long acquisition times up to 3 h were used to capture the slow dynamics of the hydrogel. In addition to a fast relaxation mode at 30 μs, there exists a slow relaxation in the range of seconds to minutes. The longest relaxation peak captured at an acquisition time of 3 h is 23 min, indicating very slow dynamics in the present hydrogel. Dynamic light scattering measurements conducted at nine different scattering angles reveal that the fast mode is diffusive (q^2-dependent) and corresponds to the cooperative diffusion of chain segments between two neighboring micellar cross-links (Figure S8). In contrast, the slow mode is q-independent, and thus, it is of structural origin. We attribute this to the slowing down of the micellar kinetics due to the interconnected micellar structure, leading to temporary fluctuations in the strength of hydrophobic associations. Figure 4d shows X-ray diffraction

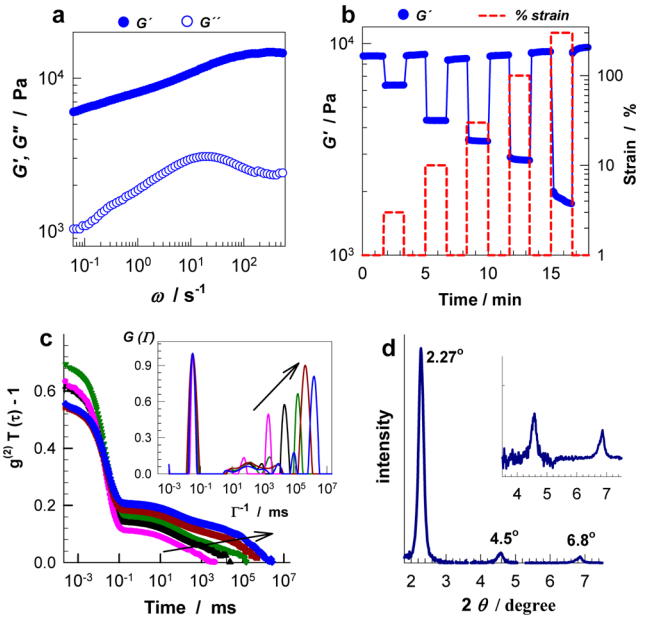

Figure 4. (a) Elastic G' and viscous moduli G'' of the hydrogel at 35 °C shown as a function of angular frequency ω. γ_0 = 0.01. (b) Five successive high−low strain cycles and the resulting moduli G'. ω = 6.3 rad s^{-1}. (c) ICFs and $G(\Gamma)$ vs relaxation time Γ^{-1} plots of the hydrogel obtained with measurement times of 30 s, 100 s, 1000 s, 1 h, and 3 h. θ = 90°. Temperature = 35 °C. The arrows show direction of increasing measurement time. (d) XRD pattern of the hydrogel. Inset: region where 2θ is 3.5°−7.5°, with an intensity scale expanded 10 times.

(XRD) pattern of the hydrogel, taken using Cu Kα radiation with λ = 0.154 nm. XRD pattern exhibits a high-intensity peak having a d-spacing of 3.9 nm and two higher angle peaks having d-spacing 2.0 and 1.3 nm. The periodical diffraction peaks indicate the existence of highly ordered supramolecular structure within the hydrogel. We attribute this to long-range ordering of the alkyl side chains of C18 M units in the water-free core of the mixed micelles.

We employed scanning force microscopy (SFM) to investigate the mobility of the gel surface and the topographic changes in response to a damage created in the hydrogel. Imaging under conditions described above, i.e., at 35 °C, was difficult due to fast, on the image acquisition time scale, changing sample topography (Figure S9). We attribute this to a high mobility of the hydrogel surface. SFM measurements conducted at ambient conditions revealed substantially higher stability of the gel surface, as described in details below. Cutting gel surface with the SFM tip by applying normal forces exceeding 1 nN readily results in trenches in gel topography (dark areas in Figure 5a). The trenches sometimes coexisted with neighboring protrusions (white areas), which we attribute to gel material pushed out or transferred by the tip onto the gel surface. Both protrusions and trenches exhibit terraced topography with a step height between 3.8 and 5.0 nm, or multiples thereof. The step height was reproducible for one particular sample but varied from sample to sample in the range from 3.8 to 5.0 nm. The smallest step height is close to the d-spacing of the hydrogel (3.9 nm). Comparison of images subsequently taken after gel cutting reveals reshaping of trenches and protrusions into circular shaped holes and islands respectively (Figure 5b, Figures S10 and S11, and Supporting Information movie). The reshaping of the structures at ambient, however, did not affect their depth, height, and

DOI: 10.1021/acs.macromol.6b00156
Macromolecules 2016, 49, 2281−2287

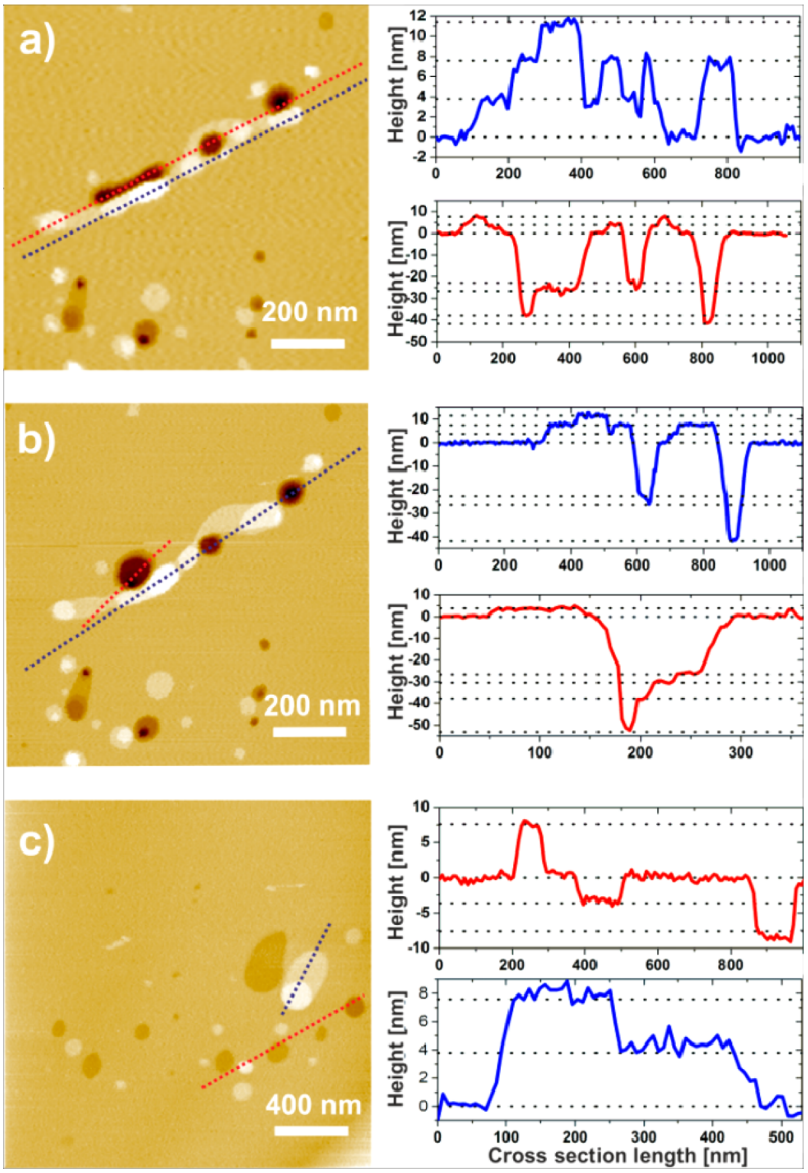

Figure 5. Topography images of gel surface taken (a) directly after cutting the surface in the upper half of the image, the holes and island in the lower part of the image are the result of the reshaping of a few previous cuts (not shown); (b) directly after the first image; and (c) after resting the sample under 35 °C and 87% RH for 1.25 h. The colored dotted lines across the images indicate the cross sections on the right side of the images in the respective colors. The surface of gel is located at the zero height on cross sections, and the dotted lines indicate steps of 3.8 nm or multiples thereof. The color scale of the images is 50 nm from black to white.

terracing of topography. The circular shape of the holes remained mostly unchanged, and their depth did not change after resting the gel samples for longer times at ambient (Figures S10 and S11). This indicates that no further remarkable changes in the hydrogel surface occur under ambient condition.

Figure 1d illustrates the mechanism we propose for the self-healing mechanism of the hydrogels. After cutting the gel sample and breaking some of the mixed micelles, the newly generated gel surface in the damaged area is in contact with air. At the air−gel interphase, surfactant molecules and polymer chains orient themselves with the hydrophilic parts toward to bulk gel phase containing 90% water while the hydrophobic parts away from the gel toward the cut surface (Figure 1d). This is actually what is observed at the water−air interface of surfactant solutions.[40] Hydrophobes that are close together at the cut surface reassociate to decrease their exposure to ambient gas phase, while SDS molecules in dynamic equilibrium with other micelles locally solubilize these associations to recover the broken mixed micelle.[17] However, the hydrophobes that are far away from each other cannot re-form the broken micelles. Thus, healing starts from the edge of the trenches so that they assume a circular shape. Moreover, both XRD and SFM results suggest that the mixed micelles acting as mobile cross-links in the hydrogel form a layered structure, like the molecules in molecular liquids. As is well-known for molecular liquids, the mobile units have fast mobility along the layers but slower mobility between the layers, yielding molecular layers with order decaying away from the surface. Under ambient conditions, the micelles should exhibit relatively fast intralayer mobility, but their interlayer motion is limited. This explains why cuts reshape into round holes while their depths remain unchanged.

DOI: 10.1021/acs.macromol.6b00156
Macromolecules 2016, 49, 2281−2287

Increasing humidity and temperature may facilitate both intra- and interlayer mobilities of the micelles. To check this, we increased the humidity (RH) and the temperature for one particular sample with the initial cut through the surface to 87% and 35 °C, respectively, with the tip retracted. We retracted the tip to avoid any possible influence of the tip on the gel dynamics. Holes and trenches of about 4−40 nm in depth and islands of about 4−12 nm in height could be detected before annealing the sample (Figure 5b). After resting the gel sample under the elevated temperature and humidity for 1.25 h, the images were taken under ambient conditions. We could not detect any more holes and islands at their initial location, yet surveying larger area revealed holes and islands 1−2 μm apart (Figure 5c). Such lateral shift substantially exceeds possible instrumental thermal drifts; therefore, we attribute it to gel dynamics. The maximum depths and heights of the holes and islands, respectively, decreased to 8 nm. After resting the same gel for another 1.25 h at 35 °C and 87% RH following imaging under ambient condition, no more islands and holes could be detected within 15 μm from their initial location. This implies that all the holes consumed the islands, and the gel sample is completely healed.

Quantitative imaging (QI) mode used to image the hydrogel samples provides elastic modulus and adhesion force images along with the height one. In all elasticity and adhesion maps, no any contrast between the surface of virgin gel, bottoms of trenches, and tops of islands was detected (Figure S12), indicating that healing recovers the original mechanical properties of the hydrogels in a nanoscale. The results thus provide a direct evidence of the effect of the intra- and interlayer mobility of mixed micelles on the progress of self-healing in micellar hydrogels. We have to mention that in macroscopic healing tests the cut surfaces of injured gel samples are pushed together to induce autonomous healing in micellar hydrogels.[17−20] This means that the spherical nanosized damage regions shown in Figure 5b are squeezed to realize self-healing. By the SFM technique, however, no force is applied to the cut surfaces to bring them together, and thus, it provides a slow-motion monitoring of a real self-healing process.

CONCLUSIONS

The addition of hydrophobic as well as hydrophilic monomers to the semidilute solution of wormlike SDS micelles leads to a conformational transition from cylindrical to spherical micelles. Before monomer addition, cryo-EM images reveal existence of several hundred nanometer long wormlike SDS micelles. SANS profiles can also be fitted to a model of wormlike micelles with a cross-sectional radius of 1.6 nm. After monomer addition, wormlike micelles completely disappear from the cryo-EM images, in favor of spherical micelles. Neutron scattering data after the monomer addition could indeed be well fitted to monodisperse spheres with a radius of 2.4 nm. After conversion of the monomers to hydrophobically modified hydrophilic polymer, the mixed micelles preserve their shape while their radius increases to 2.8 nm. The mixed micelles consisting of SDS and hydrophobic blocks of the polymer form a layered structure in the hydrogels. Self-healing tests show that the trenches and protrusions formed after gel cutting reshape into circular shaped holes and islands without affecting their depth and height. This first healing step occurring due to the intralayer mobility of mixed micelles is followed by complete healing of the hydrogel induced by interlayer mobility.

ASSOCIATED CONTENT

Supporting Information

The Supporting Information is available free of charge on the ACS Publications website at DOI: 10.1021/acs.macromol.6b00156.

Experimental details including synthesis, sample preparation, and characterization (PDF)

Reshaping of the cuts to holes (MPG)

AUTHOR INFORMATION

Corresponding Author

*(O.O.) E-mail: okayo@itu.edu.tr.

Notes

The authors declare no competing financial interest.

ACKNOWLEDGMENTS

This work was supported by Alexander von Humboldt Foundation (Georg-Forster Research Award Program) and the Scientific and Technical Research Council of Turkey (TUBITAK), KBAG 114Z312. We thank the Joint Laboratory for Structural Research, Humboldt University Berlin, for support. O.O. thanks the Turkish Academy of Sciences (TUBA) for the partial support.

REFERENCES

(1) Rehage, H.; Hoffmann, H. Viscoelastic Surfactant Solutions: Model Systems for Rheological Research. *Mol. Phys.* **1991**, *74*, 933−973.

(2) Cates, M. E.; Candau, S. J. Statics and Dynamics of Wormlike Surfactant Micelles. *J. Phys.: Condens. Matter* **1990**, *2*, 6869−6892.

(3) Cates, M. E.; Fielding, S. M. Rheology of Giant Micelles. *Adv. Phys.* **2006**, *55*, 799−879.

(4) Dreiss, C. A. Wormlike Micelles: Where do we stand? Recent Developments, Linear Rheology and Scattering Techniques. *Soft Matter* **2007**, *3*, 956−970.

(5) Jensen, G. V.; Lund, R.; Gummel, J.; Narayanan, T.; Pedersen, J. S. Monitoring the Transition from Spherical to Polymer-like Surfactant Micelles using Small-Angle X-ray Scattering. *Angew. Chem., Int. Ed.* **2014**, *53*, 11524−11528.

(6) Couillet, I.; Hughes, T.; Maitland, G.; Candau, F. Synergistic Effects in Aqueous Solutions of Mixed Wormlike Micelles and Hydrophobically Modified Polymers. *Macromolecules* **2005**, *38*, 5271−5282.

(7) Shashkina, J. A.; Phillipova, O. E.; Zaroslov, Y. D.; Khokhlov, A. R.; Pryakhina, T. A.; Blagodatskikh, I. V. Rheology of Viscoelastic Solutions of Cationic Surfactant. Effect of Added Associating Polymer. *Langmuir* **2005**, *21*, 1524−1530.

(8) Ramos, L.; Ligoure, C. Structure of a New Type of Transient Network: Entangled Wormlike Micelles Bridged by Telechelic Polymers. *Macromolecules* **2007**, *40*, 1248−1251.

(9) Yoshida, T.; Taribagil, R.; Hillmyer, M. A.; Lodge, T. P. Viscoelastic Synergy in Aqueous Mixtures of Wormlike Micelles and Model Amphiphilic Triblock Copolymers. *Macromolecules* **2007**, *40*, 1615−1623.

(10) Lee, J.-H.; Gustin, J. P.; Chen, T.; Payne, G. F.; Raghavan, S. R. Vesicle−Biopolymer Gels: Networks of Surfactant Vesicles Connected by Associating Biopolymers. *Langmuir* **2005**, *21*, 26−33.

(11) Lodge, T. P.; Taribagil, R.; Yoshida, T.; Hillmyer, M. A. SANS Evidence for the Cross-Linking of Wormlike Micelles by a Model Hydrophobically Modified Polymer. *Macromolecules* **2007**, *40*, 4728−4731.

(12) Rufier, C.; Collet, M.; Viguier, M.; Oberdisse, J.; Mora, S. SDS Interactions with Hydrophobically End-Capped Poly(ethylene oxide) Studied by ^{13}C NMR and SANS. *Macromolecules* **2009**, *42*, 5226−5235.

DOI: 10.1021/acs.macromol.6b00156
Macromolecules 2016, 49, 2281−2287

(13) Yu, L.; Ding, J. Injectable Hydrogels as Unique Biomedical Materials. *Chem. Soc. Rev.* **2008**, *37*, 1473−1481.
(14) Zhang, H.; Yu, L.; Ding, J. Roles of Hydrophilic Homopolymers on the Hydrophobic-Association-Induced Physical Gelling of Amphiphilic Block Copolymers in Water. *Macromolecules* **2008**, *41*, 6493−6499.
(15) Chen, L.; Ci, T.; Li, T.; Yu, L.; Ding, J. Effects of Molecular Weight Distribution of Amphiphilic Block Copolymers on Their Solubility, Micellization, and Temperature-Induced Sol−Gel Transition in Water. *Macromolecules* **2014**, *47*, 5895−5903.
(16) Chen, L.; Ci, T.; Yu, L.; Ding, J. Effects of Molecular Weight and Its Distribution of PEG Block on Micellization and Thermogellability of PLGA−PEG−PLGA Copolymer Aqueous Solutions. *Macromolecules* **2015**, *48*, 3662−3671.
(17) Tuncaboylu, D. C.; Sari, M.; Oppermann, W.; Okay, O. Tough and Self-healing Hydrogels Formed via Hydrophobic Interactions. *Macromolecules* **2011**, *44*, 4997−5005.
(18) Tuncaboylu, D. C.; Sahin, M.; Argun, A.; Oppermann, W.; Okay, O. Dynamics and Large Strain Behavior of Self-healing Hydrogels with and without Surfactants. *Macromolecules* **2012**, *45*, 1991−2000.
(19) Akay, G.; Hassan-Raeisi, A.; Tuncaboylu, D. C.; Orakdogen, N.; Abdurrahmanoglu, S.; Oppermann, W.; Okay, O. Self-healing Hydrogels Formed in Catanionic Surfactant Solutions. *Soft Matter* **2013**, *9*, 2254−2261.
(20) Gulyuz, U.; Okay, O. Self-healing Poly(acrylic acid) Hydrogels with Shape Memory Behavior of High Mechanical Strength. *Macromolecules* **2014**, *47*, 6889−6899.
(21) Hill, A.; Candau, F.; Selb, J. Properties of hydrophobically associating polyacrylamides: influence of the method of synthesis. *Macromolecules* **1993**, *26*, 4521−4532.
(22) Regalado, E. J.; Selb, J.; Candau, F. Viscoelastic Behavior of Semidilute Solutions of Multisticker Polymer Chains. *Macromolecules* **1999**, *32*, 8580−8588.
(23) Ghoorchian, A.; Simon, J. R.; Bharti, B.; Han, W.; Zhao, X.; Chilkoti, A.; Lopez, G. P. Bioinspired Reversibly Cross-linked Hydrogels Comprising Polypeptide Micelles Exhibit Enhanced Mechanical Properties. *Adv. Funct. Mater.* **2015**, *25*, 3122−3130.
(24) Lin, P.; Ma, S.; Wang, X.; Zhou, F. Molecularly Engineered Dual-Crosslinked Hydrogel with Ultrahigh Mechanical Strength, Toughness, and Good Self-Recovery. *Adv. Mater.* **2015**, *27*, 2054−2059.
(25) Guo, M.; Pitet, L. M.; Wyss, H. M.; Vos, M.; Dankers, P. Y. W.; Meijer, E. W. Tough Stimuli-responsive Supramolecular Hydrogels with Hydrogen-Bonding Network Junctions. *J. Am. Chem. Soc.* **2014**, *136*, 6969−6977.
(26) Collura, J. S.; Harrison, D. E.; Richards, C. S.; Kole, T. K.; Fisch, M. R. The Effects of Concentration, Pressure, and Temperature on the Diffusion Coefficient and Correlation Length of SDS Micelles. *J. Phys. Chem. B* **2001**, *105*, 4846−4852.
(27) Molchanov, V. S.; Philippova, O. E.; Khokhlov, A. R.; Kovalev, Y. A.; Kuklin, A. I. Self-Assembled Networks Highly Responsive to Hydrocarbons. *Langmuir* **2007**, *23*, 105−111.
(28) Kumar, S.; Bansal, D.; Din, K. Micellar Growth in the Presence of Salts and Aromatic Hydrocarbons: Influence of the Nature of the Salt. *Langmuir* **1999**, *15*, 4960−4965.
(29) Kunieda, H.; Ozawa, K.; Huang, K.-L. Effect of Oil on the Surfactant Molecular Curvatures in Liquid Crystals. *J. Phys. Chem. B* **1998**, *102*, 831−838.
(30) Siriwatwechakul, W.; LaFleur, T.; Prud'homme, R. K.; Sullivan, P. Effects of Organic Solvents on the Scission Energy of Rodlike Micelles. *Langmuir* **2004**, *20*, 8970−8974.
(31) Sato, T.; Acharya, D. P.; Kaneko, M.; Aramaki, K.; Singh, Y.; Ishitobi, M.; Kunieda, H. J. Oil-Induced Structural Change of Wormlike Micelles in Sugar Surfactant Systems. *J. Dispersion Sci. Technol.* **2006**, *27*, 611−616.
(32) Vogtt, K.; Siebenburger, M.; Clemens, D.; Rabe, C.; Lindner, P.; Russina, M.; Fromme, M.; Mezei, F.; Ballauff, M. A New Time-of-Flight Small-Angle Scattering Instrument at the Helmholtz-Zentrum Berlin: V16/VSANS. *J. Appl. Crystallogr.* **2014**, *47*, 237−244.
(33) The cross-sectional radius of the micelles was estimated by analyzing the scattering data in the range of q = 0.06−0.19 Å^{-1} using the Guinier approximation for the form factor[34] $qI(q) \sim \exp(-q^2R_{g,cs}{}^2/2)$, where $R_{g,cs}$ is the cross-sectional radius of gyration of the cylindrical micelles and is related to the micellar cross-sectional radius by $R = (2R_{g,cs})^{0.5}$.
(34) Koehler, R. D.; Raghavan, S. R.; Kaler, E. W. Microstructure and Dynamics of Wormlike Micellar Solutions Formed by Mixing Cationic and Anionic Surfactants. *J. Phys. Chem. B* **2000**, *104*, 11035−11044.
(35) Bastiat, G.; Grassl, B.; Francois, J. Micellar Copolymerization of Associative Polymers: Study of the Effect of Acrylamide on Sodium Dodecyl Sulfate−Poly(propylene oxide) Methacrylate Mixed Micelles. *J. Colloid Interface Sci.* **2005**, *289*, 359−370.
(36) Shibayama, M. Spatial Inhomogeneity and Dynamic Fluctuations of Polymer Gels. *Macromol. Chem. Phys.* **1998**, *199*, 1−30.
(37) Bastide, J.; Candau, S. J. In *Physical Properties of Polymeric Gels*; Cohen Addad, J. P., Ed.; Wiley: 1996; p 143.
(38) We estimated the length of a fully extended hydrocarbon chain l_{max} (in nm) by l_{max} = 0.15 + 0.1265n_c, where n_c is the number of carbon atoms in the chain.[39] For SDS micelles (n_c = 12), l_{max} is equal to 1.67 nm. Because the diameter of the sulfate headgroup is 0.5 nm,[39] a simple geometric analysis yields the radius of SDS micelles as 2.2 nm. For the mixed micelles containing C18M blocks (n_c = 17.3), similar calculations yield the micellar radius as 2.8 nm.
(39) Stokes, R. J.; Evans, D. F. *Fundamentals of Interfacial Engineering*; Wiley-VCH: 1997; p 215.
(40) Berg, J. C. *An Introduction to Interfaces & Colloids: The Bridge to Nanoscience*; World Scientific: Singapore, 2010.

DOI: 10.1021/acs.macromol.6b00156
Macromolecules 2016, 49, 2281−2287